Physics Letters B 719 (2013) 394–398

Contents lists available at SciVerse ScienceDirect

Physics Letters B

www.elsevier.com/locate/physletb

Ultra-relativistic nuclear collisions: Event shape engineering

Jürgen Schukraft [a], Anthony Timmins [b], Sergei A. Voloshin [c,*]

[a] PH Division, CERN, CH-1211 Geneva 23, Switzerland
[b] University of Houston, Houston, TX 77204, United States
[c] Wayne State University, 666 W. Hancock, Detroit, MI 48201, United States

ARTICLE INFO

Article history:
Received 30 August 2012
Received in revised form 13 January 2013
Accepted 21 January 2013
Available online 24 January 2013
Editor: J.-P. Blaizot

ABSTRACT

The evolution of the system created in a high energy nuclear collision is very sensitive to the fluctuations in the initial geometry of the system. In this Letter we show how one can utilize these large fluctuations to select events corresponding to a specific initial shape. Such an "event shape engineering" opens many new possibilities in quantitative test of the theory of high energy nuclear collisions and understanding the properties of high density hot QCD matter.

Many features of multiparticle production in ultra-relativistic nuclear collisions reflect the initial collision geometry of the system. These initial conditions affect to a different degree all the particles and therefore lead to truly multiparticle effects usually referred to as anisotropic collective flow. Studying anisotropic flow in nuclear collisions provides unique and invaluable information about the evolution of the system created in a collision, properties of high density hot QCD matter, and the physics of multiparticle production in general [1,2]. Even at fixed impact parameter, i.e. for fixed average collision geometry, the position of the individual interacting nucleons fluctuates event by event, which leads to fluctuations in the initial shape of the nuclear overlap region [3,4]. Recently, significant progress has been made in understanding the role of the fluctuations in the initial density distribution [5–9]. In particular it was realized that such fluctuations lead to odd harmonic anisotropic flow, which enable new insights into the dynamics of the system evolution. The experimental measurements [10,11] confirm the existence of collective flow up to at least sixth harmonic, thus lending strong support to the picture.

At present, the effect of the initial geometry on final state observables can be studied only by varying the collision centrality, or colliding nuclei of different size and shape. It has been always tempting to study anisotropic flow at maximum particle density that is reached in very central collisions. However the average anisotropies in central collisions are small. Collisions of very non-spherical nuclei, such as uranium, should be able to provide events with large initial anisotropy and high particle density (in the so-called body–body collisions), however the analysis might be very complicated due to a large variety of possible overlap geometries that have to be experimentally disentangled. In this Letter we discuss how one can utilize the strong event-by-event fluctuations in the initial geometry to select events with different initial system shapes even at fixed impact parameter, e.g. central Au + Au collisions with either large or small initial anisotropy, and in this way study the system evolution under conditions not possible before.

The study of particle production in events corresponding to a specific geometry opens a number of very attractive possibilities. One of those, mentioned above, is the study of the system evolution in a high density regime (central collisions) and concurrently strongly anisotropic initial conditions. This would add new constraints to questions such as how close the system is to the so-called "hydrodynamic limit" and the development of the anisotropic flow velocities fields. Analysis of transverse momentum spectra in events with fixed particle density but varying geometrical deformation can shed light on the correlation between radial and anisotropic flow. Another example would be understanding the "away-side" double bump structure in two-particle azimuthal correlations [12,13]. Several years ago, this attracted a considerable attention as a possible indication of the Mach cone due to propagation of a very energetic parton through the dense medium. More recently it was found that this structure is likely due to triangular (third harmonic) flow. Additional proof for this interpretation might come from studying such correlations in events with very small triangularity. Several other examples, including azimuthally sensitive femtoscopy and an estimate of the background effects in chiral magnetic effect studies will be discussed later in the Letter.

There might be different approaches to s classify individual events according to their geometrical deformation, i.e. to perform an event shape engineering (ESE). The one adopted in this Letter is an extension of the technique proposed in [14] that is based on the event selection according to the magnitude of the so-called reduced flow vector q_n (the subscript n is the harmonic number,

* Corresponding author.
E-mail address: voloshin@wayne.edu (S.A. Voloshin).

0370-2693
http://dx.doi.org/10.1016/j.physletb.2013.01.045

for the exact definitions see below). We always perform ESE using two subevents. We use here a common terminology in flow analyses, where a subevent refers to a distinct subset of all measured particles selected either at random or in a given rapidity and/or transverse momentum region. One of the subevents is used to select events according to their shape (we will always call it subevent "a" below) whereas the physical analysis of any event properties is performed on the second subevent (subevent "b"). Using two subevents helps to avoid nonphysical biases due to nonflow effects as discussed below. The second subevent (subevent "b") is also used to extract the average flow value and its fluctuations in the selected event sample, as the unknown nonflow contribution to the q_n-distribution used for the event selection prohibits such an evaluation based solely on subevent "a". We use the Monte Carlo Glauber model to illustrate how the event selection based on flow vectors works and outline the general scheme for the corresponding experimental analysis.

To quantify the anisotropic flow we use a standard Fourier decomposition of the azimuthal particle distribution with respect to the n-th harmonic symmetry planes [15,16]:

$$E\frac{d^3N}{d^3p} = \frac{1}{2\pi}\frac{d^2N}{p_T\,dp_T\,dy}\left(1+\sum_{n=1}^{\infty}2v_n\cos\left[n(\phi-\Psi_n)\right]\right), \tag{1}$$

where v_n is the n-th harmonic flow coefficient and Ψ_n is the n-th harmonic symmetry plane determined by the initial geometry of the system (as given by the participant nucleon distribution, see below). The event-by-event fluctuations in anisotropic flow are believed to follow the fluctuations in the corresponding eccentricities of the initial density distribution. Following [9], for the latter we use the definition

$$\varepsilon_{n,x} = \left\langle r^n\cos(n\phi)\right\rangle, \qquad \varepsilon_{n,y} = \left\langle r^n\sin(n\phi)\right\rangle, \tag{2}$$

$$\varepsilon_{n,p} = \sqrt{\varepsilon_{n,x}^2+\varepsilon_{n,y}^2}, \qquad \tan(n\Psi_n) = \varepsilon_{n,y}/\varepsilon_{n,x}, \tag{3}$$

where $\varepsilon_{n,p}$ is the so-called *participant* eccentricity [4]. The average can be taken with energy or entropy density as a weight. In our Monte Carlo model we weight with the number of participating nucleons (those undergoing inelastic collision). For the nucleon distribution in the nuclei we use the Woods–Saxon density distribution with standard parameters (for the exact values see [14]); the inelastic nucleon–nucleon cross section is taken to be 64 mb. We assume that the flow values are proportional to the corresponding eccentricities with the ratio fixed to approximately reproduce measured v_n values [11]. As it is shown in [17], in this case the distribution in v_n is very well described by the so-called Bessel–Gaussian (BG) distribution

$$p(v) = \mathrm{BG}(v; v_0, \sigma_{vx}), \tag{4}$$

where

$$\mathrm{BG}(x; x_0, \sigma) \equiv \frac{x}{\sigma}I_0\left(\frac{x_0x}{\sigma^2}\right)\exp\left(-\frac{x_0^2+x^2}{2\sigma^2}\right), \tag{5}$$

which is the radial projection of a 2-dimensional Gaussian distribution with width σ in each dimension and shifted off the origin by a distance x_0.

The flow vectors are calculated in two subevents [1,16] with multiplicities in each subevent approximately corresponding to $\Delta\eta = 0.8$ in Pb + Pb collisions at LHC energies [18] (approximately 1200 charged particles per subevent for 0–5% centrality). The multiplicities are generated with a negative binomial distribution based on the number of participants and the number of binary collision as in [14], using about 1.2 M simulated events for each 5% bin in centrality.

The flow vectors are defined as

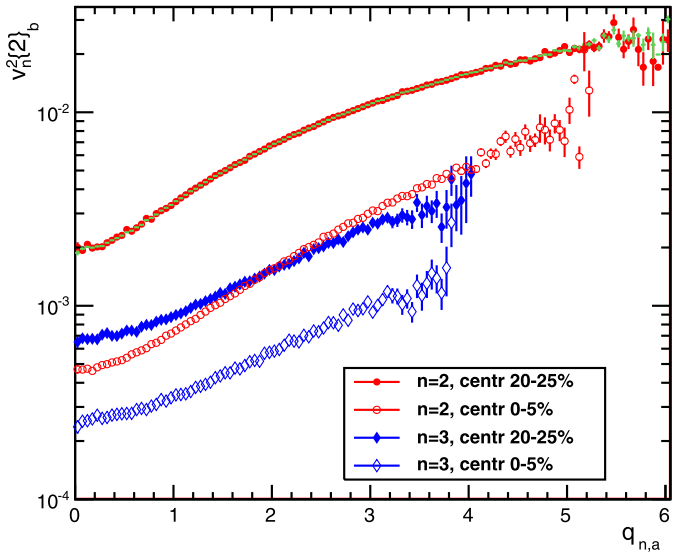

Fig. 1. (Color online.) Mean elliptic and triangular flow values in a-subevent as function of the corresponding q_n magnitude in b-subevent for two different centrality selections.

$$Q_{n,x} = \sum_i^M \cos(n\phi_i), \qquad Q_{n,y} = \sum_i^M \sin(n\phi_i), \tag{6}$$

$$q_n = Q_n/\sqrt{M}, \tag{7}$$

$$q_n^2 = 1 + (M-1)\left\langle\cos\left[n(\phi_i-\phi_j)\right]\right\rangle_{i\neq j} \tag{8}$$

where M is the particle multiplicity and ϕ_i are the azimuthal angles of particles in a given subevent. Eq. (8) presents the relation between the length of the q_n vector and the average correlation between all pairs of particles in a given event. The distribution in the magnitude of flow vectors q_n, which are measured event by event, has been proposed [15] and often used to measure the average flow [1,19]. The distribution in q_n is determined by the v_n distribution convoluted with statistical fluctuations due to the finite particle multiplicity (plus any detector resolution effects, if relevant). For relatively high multiplicities ($M \gtrsim 300$) it is also very well described by a BG distribution

$$p(q) = \mathrm{BG}(q; q_0, \sigma_{qv}) \tag{9}$$

with parameters directly related to those of the underlying v_n distribution:

$$q_0 = \sqrt{M}v_0, \qquad \sigma_{qv}^2 = \sigma_{qx}^2 + M\sigma_{vx}^2, \tag{10}$$

$$\sigma_{qx}^2 = \frac{1}{2}[1+M\delta], \tag{11}$$

where M is the multiplicity used to build the flow vector, and the nonflow parameter δ accounts for possible correlations not related to the initial geometry of the system. (For a more detailed discussion of the functional form of q_n distributions see [20].) Thus, the fit to the q_n-distribution provides information to both the average flow value as well as flow fluctuations, *if* the nonflow contribution can be neglected or estimated from other measurements. On average, q values are larger in events with larger flow, which allows to use q-distributions for selection of the events with large or small flow.

1. Zero nonflow

We start the discussion of the ESE with the simplest case when all the correlations in the system are determined only by

anisotropic flow. Fig. 1 shows the average values of v_n^2 $(n = 2, 3)$ calculated via the 2-particle correlation method in one of the subevents ("b") as function of the flow vector magnitude in the second subevent ("a"). In the simulations the two subevents are statistically independent and are correlated only via the common participant plane and flow values. Therefore the results $v_{n,b}^2\{2\}$ extracted for subevent "b" correspond on average to the "true" values of $\langle v_n^2 \rangle$ for the given event sample. The results in Fig. 1 demonstrate that within a narrow centrality bin one can select event classes with average flow values varying by more than a factor of two, based on the magnitude of the reduced flow vector.

When separating events according to their flow values, not only the mean flow values in each event class are relevant but also the width of the flow distribution in each class (and therefore the overlap between classes). The latter depends on the "experimental resolution" of the event-by-event flow, which increases with the number of particles used to calculate the flow vector, as well as depends, more weakly, on the flow magnitude itself. We find that for a multiplicity corresponding in our example to centrality 20–25%, the width of the v_2 distribution for a fixed $q_{2,a}$ value is about factor of 1.5 smaller than that for the unbiased event sample (changing from 0.031 to 0.022); the width decreases by about 20% if one doubles the size of the subevent (double the multiplicity) used for the q_2 determination.

In practice one can obtain information about the v_n distributions in any given event class, corresponding to different cuts on the $q_{n,a}$ values, from the fits to the $q_{n,b}$-distributions. Fig. 2 shows distribution in $q_{n,b}$ (subevent-b) for three different selections on $q_{n,a}$, separately for the second and third harmonic flow components. The selections correspond to the full unbiased distribution (no cuts) and the 5% lowest and 5% highest $q_{n,a}$ values, respectively. All $q_{n,b}$ distributions in Fig. 2 are fit to the BG functional form to extract the corresponding mean flow values and the corresponding width (see, e.g. [1]). It is remarkable that the fits are very good not only for the unbiased q-distributions but also for the ones corresponding to the low flow and high flow "engineered events". Using the extracted fit parameters we plot the corresponding v_n distributions in Fig. 3 (shown by dashed lines) and compare them to the actual ("true") v_n distributions (shown as a histogram), which are known in the Monte Carlo simulation. One finds an excellent agreement between the two indicating both that the v_n distributions in the "shape engineered" events are also very close to a BG form and that the full distribution of flow values in each selected event class can be very well approximated from fits to the corresponding q-distribution. Indeed, we have found that in the Gaussian approximation [17], the conditional probability density $p(v_n|q_n)$ (v_n probability density in events with given q_n) is given by following equation:

$$p(v|q) = \frac{p(v)p(q|v)}{p(q)} \tag{12}$$

$$= \frac{\mathrm{BG}(v; v_0, \sigma_{vx})\mathrm{BG}(q; \sqrt{M}v, \sigma_{qx})}{\mathrm{BG}(q; \sqrt{M}v_0; \sigma_{qv})}, \tag{13}$$

where the subscript n is omitted for clarity. It appears that for realistic values of the parameters this equation is very well approximated by a single BG function, which explains the possibility to fit the distributions shown in Fig. 2 to the BG form.

2. Nonflow effects

The ESE approach described above is based on using two subevents. In this case possible nonflow effects can be separated in two major categories (a) when nonflow effects are present within each of the subevents, but there is no nonflow correlations between subevents "a" and "b", and (b) when nonflow correlations are present between, as well as within, subevents. We do not know a good solution to the case (b) and below we only discuss possible biases in the event selection one might expect in this case. In a real analysis one should try to minimize the nonflow correlations between the two subevents which are used for ESE selection and physical analysis, respectively. A practical solution to that might be to use subevents which are separated by a significant (pseudo)rapidity gap.

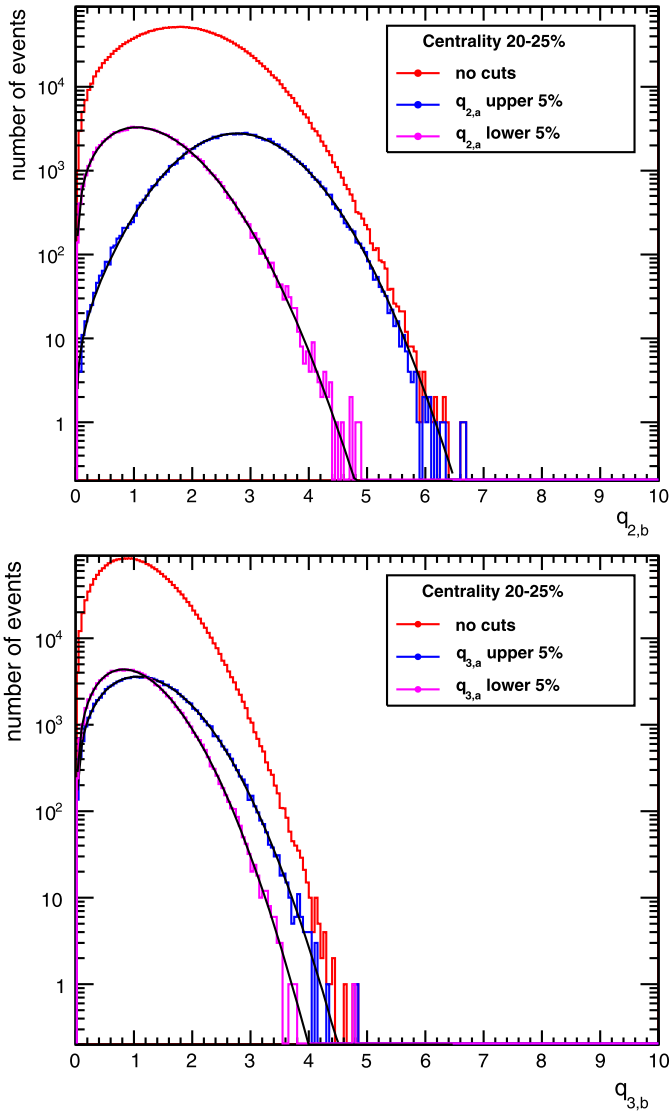

Fig. 2. (Color online.) $q_{2,b}$ and $q_{3,b}$ distributions in the event samples selected by different cuts on the corresponding $q_{n,a}$-vector magnitude indicated in the plot. The lines show the BG fit to the distribution.

The case (a) can be addressed by the conventional flow analysis. After the event selection is done with $q_{n,a}$ cuts, and the flow in the selected events can be estimated using particles in subevent "b" with standard methods, including e.g. many-particle cumulant analysis [21–23]. Note that in case (a) the two subevents are correlated only via the strength of flow (i.e. the value of the initial eccentricity), and therefore any potential effect introduced by nonflow into the event selection made with $q_{n,a}$ will not bias the flow measurement in subevent "b".

To demonstrate possible biases to the analysis in case (b), we introduce nonflow into our Monte Carlo Glauber model. Nonflow effects are simulated by assuming that a fraction (in this simu-

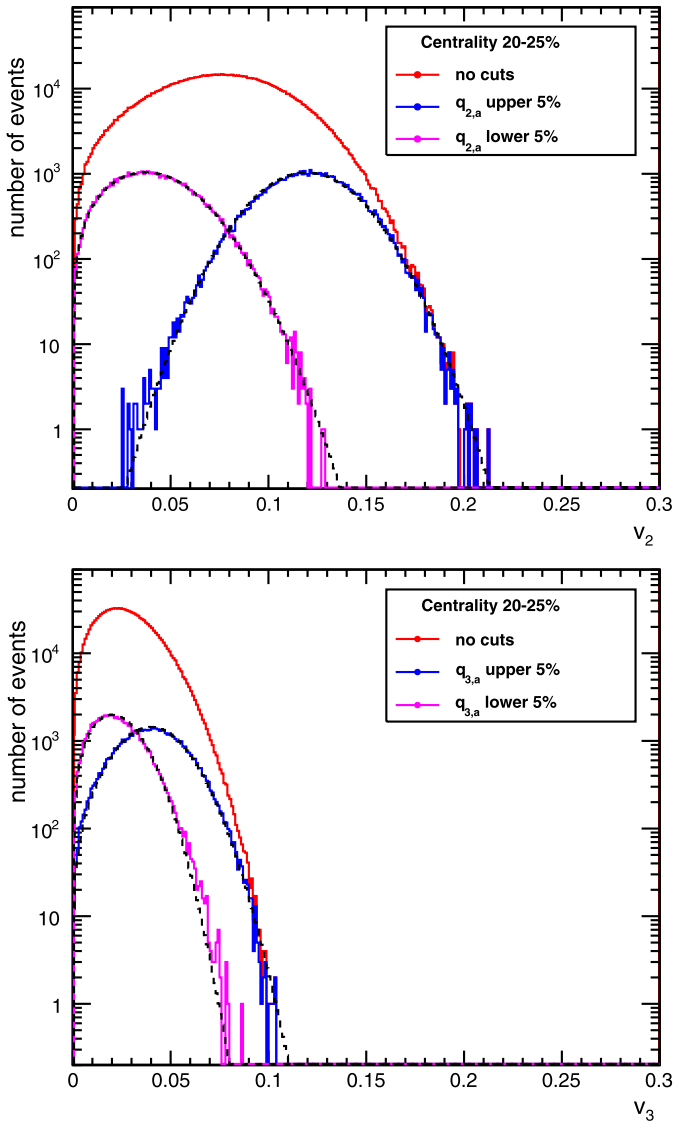

Fig. 3. (Color online.) Actual (true) v_2 and v_3 distributions in the event samples selected by different cuts on the corresponding q_n-vector magnitude indicated in the plot, compared to that extracted from the BG fits to $q_{n,b}$ distribution shown in Fig. 2 (dashed lines). Note that the lines are not fits to the histograms!

lation half) of all particles in the entire event are produced in pairs with both particles in a pair emitted with the same azimuthal angle [22]. Each particle is assigned randomly to one of the two subevents. In this case the nonflow parameter δ is of size $\delta = 1/(2M)$, where M is the (full) event multiplicity, which roughly corresponds to the nonflow estimates at the LHC energies. Fig. 4 presents the results for the flow calculation in subevent "a" using 2- and 4-particle cumulant methods as function of $q_{2,b}$. The expectations based on simulated flow are also shown. One observes a significant bias due to nonflow, leading to an overestimate of the flow values in high flow selected events and an underestimate in the low flow selected events. This trend is due to positive sign of the nonflow correlations. The bias in the corresponding v distributions is shown in Fig. 5. Note that even though the bias of the mean values of flow is modest, at large values of v_n the actual distribution differs by orders of magnitude from the one deduced from the q-distribution fits.

Below we discuss briefly several analyses which can profit from event shape engineering.

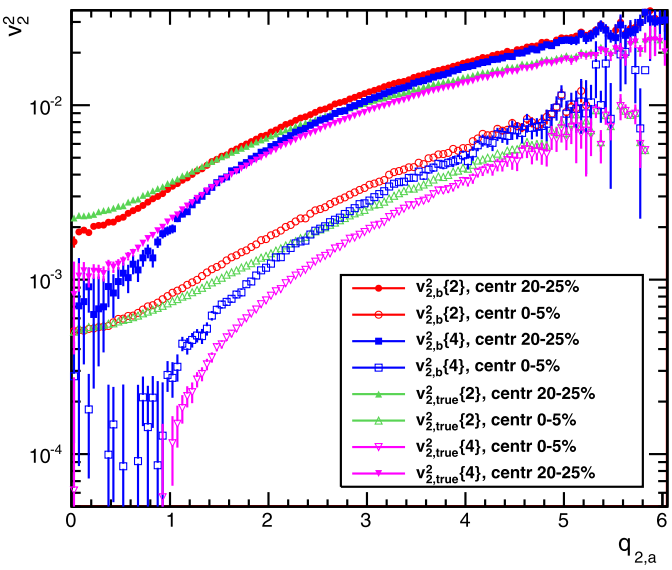

Fig. 4. (Color online.) Elliptic flow measured with 2- (red points) and 4-particle (blue) cumulant method in subevent "b" as a function of the corresponding $q_{2,a}$ magnitude. Solid symbols correspond to centrality 20–25%, and open symbols to 0–5% centrality. The true (simulated) values are shown by green markers, as expected for 2-particle cumulant results and by magenta for 4-particle cumulant results.

3. The chiral magnetic effect

The chiral magnetic effect proposed in [24–26] is a charge separation along the magnetic field. If observed it would manifest local parity violation in the strong interaction. A correlator sensitive to the CME was proposed in Ref. [27]:

$$\langle \cos(\phi_\alpha + \phi_\beta - 2\Psi_{RP}) \rangle, \tag{14}$$

where subscripts α, β denote the particle type. STAR [28,29], as well as ALICE [30] measurements of this correlator are consistent with the expectation for the CME. An ambiguity in the interpretation of experimental results comes from a possible background of reaction plane dependent correlations not related to CME. Note that a key ingredient to CME is the strong magnetic field, while all the background effects originate from elliptic flow [27]. This can potentially be used to experimentally resolve the question. One possibility is to study the effect in central collisions of non-spherical uranium nuclei [14], where the relative contributions of the background (proportional to the elliptic flow) and the CME (proportional to the magnetic field) should be very different in tip-tip and body–body type collisions. The second possibility would be to exploit the large flow fluctuations in heavy-ion collisions as discussed in [14,31] and ESE would be a technique to perform such an analysis. (Note that the magnetic field depends very weakly on the initial geometry fluctuations [31].) Yet another test, proposed in [32], is based on the idea that the charge separation along the magnetic field should be zero if measured with respect to the 4-th harmonic event planes, while the background effects due to flow should still be present, albeit smaller in magnitude ($\sim v_4$). An example of such a correlator, would be $\langle \cos(2\phi_\alpha + 2\phi_\beta - 4\Psi_4 \rangle$, where Ψ_4 is the fourth harmonic event plane. The value of the background due to flow could be estimated by rescaling the correlator Eq. (14). Such measurements will require good statistics, and *strong* fourth harmonic flow. Again, ESE can be very helpful to vary any effects related to flow.

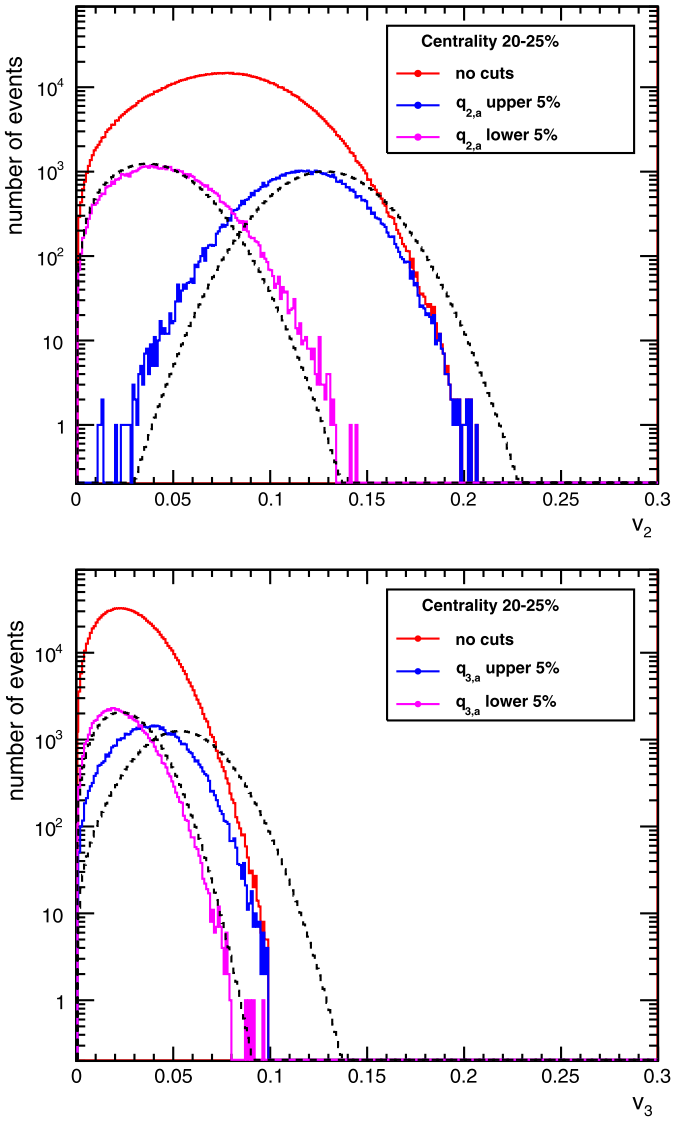

Fig. 5. (Color online.) The same as in Fig. 3 but for the case of nonflow described in the text.

4. Measuring the shape and freeze-out velocity profile with azimuthally sensitive femtoscopy

Different shapes in the initial geometry of the collision will be preserved to some degree in the system freeze-out shapes. It was shown in [33] that those shapes can be measured experimentally with azimuthally sensitive femtoscopic analysis [34,35]. Such an analysis would definitely profit from events with extreme values of anisotropy provided by ESE, as the variation of femtoscopic parameters with azimuth would be more pronounced. General details of femtoscopic analyses and discussion of the experimental results can be found in a review [36].

5. Summary

Event shape engineering, providing the possibility to select and study events corresponding to nuclear collisions with different initial geometry configuration, promises to be a very useful new tool to study the properties of the strongly interacting matter in ultra-relativistic heavy ion collisions.

Acknowledgements

The authors are indebted to our colleagues at the ALICE Collaboration for numerous fruitful discussion. The work of A.T. and S.V. was supported in part by the U.S. Department of Energy under Contracts DE-FG02-92ER41512 and DE-FG02-92ER40713.

References

[1] S.A. Voloshin, A.M. Poskanzer, R. Snellings, in: Landolt–Boernstein, Relativistic Heavy Ion Physics, vol. 1/23, Springer-Verlag, 2010, pp. 5–54.
[2] B. Muller, J. Schukraft, B. Wyslouch, arXiv:1202.3233 [hep-ex].
[3] M. Miller, R. Snellings, nucl-ex/0312008.
[4] B. Alver, et al., PHOBOS Collaboration, Phys. Rev. Lett. 98 (2007) 242302, nucl-ex/0610037.
[5] A.P. Mishra, R.K. Mohapatra, P.S. Saumia, A.M. Srivastava, Phys. Rev. C 77 (2008) 064902.
[6] P. Sorensen, arXiv:0905.0174 [nucl-ex].
[7] J. Takahashi, et al., Phys. Rev. Lett. 103 (2009) 242301.
[8] B. Alver, G. Roland, Phys. Rev. C 81 (2010) 054905;
B. Alver, G. Roland, Phys. Rev. C 82 (2010) 039903 (Erratum).
[9] D. Teaney, L. Yan, arXiv:1010.1876 [nucl-th].
[10] K. Aamodt, et al., ALICE Collaboration, Phys. Rev. Lett. 105 (2010) 252302.
[11] K. Aamodt, et al., ALICE Collaboration, Phys. Rev. Lett. 107 (2011) 032301, arXiv:1105.3865 [nucl-ex];
G. Aad, et al., ATLAS Collaboration, Phys. Rev. C 86 (2012) 014907, arXiv:1203.3087 [hep-ex];
A. Adare, et al., PHENIX Collaboration, Phys. Rev. Lett. 107 (2011) 252301, arXiv:1105.3928 [nucl-ex];
M. Issah, CMS Collaboration, AIP Conf. Proc. 1422 (2012) 50;
P. Sorensen, STAR Collaboration, J. Phys. G 38 (2011) 124029, arXiv:1110.0737 [nucl-ex].
[12] J. Adams, et al., STAR Collaboration, Phys. Rev. Lett. 95 (2005) 152301, nucl-ex/0501016.
[13] A. Adare, et al., PHENIX Collaboration, Phys. Rev. C 78 (2008) 014901, arXiv:0801.4545 [nucl-ex].
[14] S.A. Voloshin, Phys. Rev. Lett. 105 (2010) 172301, arXiv:1006.1020 [nucl-th].
[15] S. Voloshin, Y. Zhang, Z. Phys. C 70 (1996) 665.
[16] A.M. Poskanzer, S.A. Voloshin, Phys. Rev. C 58 (1998) 1671.
[17] S.A. Voloshin, A.M. Poskanzer, A. Tang, G. Wang, Phys. Lett. B 659 (2008) 537, arXiv:0708.0800 [nucl-th].
[18] K. Aamodt, et al., ALICE Collaboration, Phys. Rev. Lett. 106 (2011) 032301, arXiv:1012.1657 [nucl-ex].
[19] J. Adams, et al., STAR Collaboration, Phys. Rev. C 72 (2005) 014904, nucl-ex/0409033.
[20] P. Sorensen, STAR Collaboration, J. Phys. G 35 (2008) 104102, arXiv:0808.0356 [nucl-ex].
[21] N. Borghini, P.M. Dinh, J.-Y. Ollitrault, Phys. Rev. C 64 (2001) 054901, nucl-th/0105040.
[22] C. Adler, et al., STAR Collaboration, Phys. Rev. C 66 (2002) 034904, nucl-ex/0206001.
[23] A. Bilandzic, R. Snellings, S. Voloshin, Phys. Rev. C 83 (2011) 044913, arXiv:1010.0233 [nucl-ex].
[24] D. Kharzeev, Phys. Lett. B 633 (2006) 260.
[25] D. Kharzeev, A. Zhitnitsky, Nucl. Phys. A 797 (2007) 67.
[26] D.E. Kharzeev, L.D. McLerran, H.J. Warringa, Nucl. Phys. A 803 (2008) 227.
[27] S.A. Voloshin, Phys. Rev. C 70 (2004) 057901.
[28] B.I. Abelev, et al., STAR Collaboration, Phys. Rev. Lett. 103 (2009) 251601.
[29] B.I. Abelev, et al., STAR Collaboration, Phys. Rev. C 81 (2010) 054908.
[30] B. Abelev, et al., ALICE Collaboration, arXiv:1207.0900 [nucl-ex].
[31] A. Bzdak, arXiv:1112.4066 [nucl-th].
[32] S.A. Voloshin, Prog. Part. Nucl. Phys. 67 (2012) 541, arXiv:1111.7241 [nucl-ex].
[33] S.A. Voloshin, J. Phys. G 38 (2011) 124097, arXiv:1106.5830 [nucl-th].
[34] S.A. Voloshin, W.E. Cleland, Phys. Rev. C 53 (1996) 896, nucl-th/9509025;
S.A. Voloshin, W.E. Cleland, Phys. Rev. C 54 (1996) 3212, nucl-th/9606033.
[35] S. Voloshin, R. Lednicky, S. Panitkin, N. Xu, Phys. Rev. Lett. 79 (1997) 4766, nucl-th/9708044.
[36] M.A. Lisa, S. Pratt, R. Soltz, U. Wiedemann, Ann. Rev. Nucl. Part. Sci. 55 (2005) 357.